Queensland University of Technology
Brisbane Australia

This is the author's version of a work that was submitted/accepted for publication in the following source:

Pologanathan, Keerthan & Mahendran, Mahen
(2015)
Improved shear design rules of cold-formed steel beams.
Engineering Structures, *99*, pp. 603-615.

This file was downloaded from: http://eprints.qut.edu.au/87026/

© Copyright 2015 Elsevier Ltd. All rights reserved.

Notice: *Changes introduced as a result of publishing processes such as copy-editing and formatting may not be reflected in this document. For a definitive version of this work, please refer to the published source:*

http://doi.org/10.1016/j.engstruct.2015.04.027

Improved Shear Design Rules of Cold-formed Steel Beams

Poologanathan Keerthan and Mahen Mahendran

Science and Engineering Faculty

Queensland University of Technology, Brisbane, QLD 4000, Australia

Abstract: Light gauge cold-formed steel sections have been developed as more economical building solutions to the alternative heavier hot-rolled sections in the commercial and residential markets. Cold-formed lipped channel beams (LCB), LiteSteel beams (LSB) and triangular hollow flange beams (THFB) are commonly used as flexural members such as floor joists and bearers while rectangular hollow flange beams (RHFB) are used in small scale housing developments through to large building structures. However, their shear capacities are determined based on conservative design rules. For the shear design of cold-formed steel beams, their elastic shear buckling strength and the potential post-buckling strength must be determined accurately. Hence experimental and numerical studies were conducted to investigate the shear behaviour and strength of LCBs, LSBs, THFBs and RHFBs. Improved shear design rules including the direct strength method (DSM) based design equations were developed to determine the ultimate shear capacities of these open and hollow flange steel beams. An improved equation for the higher elastic shear buckling coefficient of cold-formed steel beams was proposed based on finite element analysis results and included in the design equations. A new post-buckling coefficient was also introduced in the design equations to include the available post-buckling strength of cold-formed steel beams. This paper presents the details of this study on cold-formed steel beams subject to shear, and the results. It proposes generalised and improved shear design rules that can be used for any type of cold-formed steel beam.

Keywords: Cold-formed steel structures, Lipped channel beams, Hollow flange beams, Elastic shear buckling, Post buckling, Experiments, Numerical studies and Direct strength method.

Corresponding author's email address: m.mahendran@qut.edu.au

1. Introduction

In recent times cold-formed steel members have become an increasingly integral part of the construction and building industries. They have many advantages over other construction materials including their light weight, high strength, high quality, protection, cost effective fabrication and non-combustibility. They are used in applications such as building frames, roof trusses, purlins and girts, floor framing and many other load bearing components.

Since early 1990s, Australian companies such as OneSteel Australian Tube Mills [1] have produced innovative cold-formed hollow flange sections known as the doubly symmetric Triangular Hollow Flange Beams (THFB) and the monosymmetric LiteSteel Beams (LSB) with rectangular hollow flanges (see Figure 1). The development of these sections was based on improving the structural efficiency by adopting torsionally rigid hollow flanges, minimising local buckling of plate elements by eliminating free edges, distributing material away from the neutral axis to afford greater bending stiffness than conventional cold-formed sections, and optimising manufacturing efficiency. These hollow flange sections were produced from a single steel strip using a combined dual electric resistance welding and automated continuous roll-forming process. This manufacturing process produces higher yield strengths for the sections' plate elements, in particular for flange elements.

Rectangular hollow flange beams (RHFB) are also new steel members, consisting of cold-formed rectangular hollow sections for both the top and bottom flanges welded to a flat web plate (see Figure 1). They can also be cold-formed and welded or screw/rivet fastened along the web-flange juncture. The doubly symmetric RHFBs can be used as long spanning flexural members in various applications. Figure 1 shows the hollow flange sections (THFB, LSB and RHFB) and one of the commonly used open cold-formed sections known as lipped channel beam (LCB). It also includes a monosymmetric THFB section.

In steel building systems, LCBs, LSBs, THFBs and RHFBs can be used as flexural members, for example, floor joists and bearers. For these cold-formed steel beams to be used as flexural members, their flexural and shear capacities must be known accurately including the potential post-buckling strength. In relation to shear capacity calculations, the elastic shear buckling coefficients of web panels are determined by assuming conservatively that the web panels are simply supported at the junction between the flange and web elements, and ignoring any post-

buckling strength. In the traditional shear design method of cold-formed steel beams, the web shear buckling performance is considered without the effect of flange rigidity. The shear strength of cold-formed steel LCBs was studied by LaBoube and Yu [2]. They determined the ultimate strengths of LCBs by assuming that the web-flange juncture of LCBs was simply supported. Aswegan and Moen [3] investigated the elastic shear buckling stresses of C- and Z-Sections using hand solutions. Pham and Hancock [4] investigated the elastic buckling behaviour of unlipped and lipped channel section members subject to shear using an isoparametric spline finite strip method. They found that the flanges can have a significant influence on the shear buckling capacity of thin-walled channel sections. However, they did not propose a simple equation to determine the shear buckling coefficients of LCBs.

Pham and Hancock [5] conducted both experimental and numerical studies to investigate the shear behaviour of high strength cold-formed steel lipped channel sections. Suitable design equations for the shear capacity of LCBs (Equations 1 and 2) were then proposed in Pham and Hancock [6]. These shear design equations have also been adopted in AISI S100 [7]. These equations predict the shear strength of LCBs which include their available post-buckling strength and the effect of additional fixity at the web-flange juncture. In these equations the DSM based nominal shear capacity (V_v) is proposed based on V_{cr} (elastic buckling capacity in shear) and V_y (shear yield capacity).

$$V_v = V_y \qquad \text{for} \quad \frac{d_1}{t_w} \le \sqrt{\frac{Ek_v}{f_{yw}}} \tag{1}$$

$$V_V = \left[1 - 0.15\left(\frac{V_{cr}}{V_y}\right)^{0.4}\right]\left(\frac{V_{cr}}{V_y}\right)^{0.4} V_y \qquad \text{for} \quad \frac{d_1}{t_w} > \sqrt{\frac{Ek_v}{f_{yw}}} \tag{2}$$

$$V_v = V_y = 0.6\, f_{yw} d_1 t_w \tag{3}$$

$$V_v = V_{cr} = \frac{k_v \pi^2 E t_w^3}{12\left(1-\nu^2\right) d_1} \tag{4}$$

where k_v is the enhanced elastic shear buckling coefficient of channel sections and its values are given in Pham [6].

Although various studies have been conducted on LSBs subject to pure bending [8,9], research related to their shear capacities are limited [10,11]. Keerthan and Mahendran [12-14] investigated the elastic shear buckling behaviour of LSBs and LCBs. They proposed simple equations for the determination of elastic shear buckling coefficients of LSBs and LCBs. They found that the realistic support condition of LCB at the web-flange juncture is closer to a simply supported condition while that of LSB is closer to a fixed supported condition. However there are no simple equations to determine the shear buckling coefficients of RHFBs and THFBs. Hence in this research the elastic shear buckling behaviour of RHFBs and THFBs was investigated using finite element analyses (FEA) including the effect of true support conditions at the junction between their flange and web elements. These finite element models included idealized simply supported boundary conditions and a shear flow based loading to prevent any torsional effect. For comparison purposes, a plate girder (PG) was also considered in FEA. The results were then used to develop an equation for the elastic shear buckling coefficient of these beams and determine the corresponding ultimate shear capacity improvement based on the direct strength method (DSM) based shear capacity equations proposed by Keerthan and Mahendran [13].

An increased shear buckling coefficient (k_v) and a post-buckling coefficient (p_n) were also introduced in the DSM based shear capacity equations to allow for the additional fixity in the web-flange juncture instead of k_v assumed as 5.34 in AS/NZS 4600 [15] and include the available post-buckling strength of cold-formed steel beams, respectively. These two coefficients depend on the type of steel beam section. The ultimate shear capacities of any open and hollow flange cold-formed steel beams can be computed using the proposed DSM based shear capacity equations if the relevant elastic shear buckling coefficient (k_v) and post-buckling coefficient (p_n) are known. This paper presents the details of this study including finite element models, shear buckling modes and coefficients and DSM based shear capacity equations including both the increased shear buckling and post-buckling strengths. It also includes the results of LSBs and LCBs based on Keerthan and Mahendran [13,14].

2. Elastic Shear Buckling Analyses

2.1. Model Description

This section presents the development of finite element models to investigate the shear behaviour of hollow flange (LSBs, THFBs and RHFBs) and open (LCBs and PG) steel beams

including their elastic shear buckling characteristics. For this purpose, a simply supported beam with a mid-span load was considered. A general purpose finite element program ABAQUS [16], which has the capability of undertaking geometric and material non-linear analyses of three dimensional structures, was used. Idealized simply supported boundary conditions were implemented in the beams under a three point loading arrangement. Figure 2 shows the schematic diagram of the loading set-up used in this research. An aspect ratio (a/d_1) of 1.0 was used to simulate a primarily shear behaviour. ABAQUS has several element types to simulate the shear behaviour of beams. But among those, shell element was selected as it has the capability to simulate the shear buckling behaviour of LSBs, LCBs, THFBs, RHFBs and PGs. The shell element available in ABAQUS called S4R was used to model the shear behaviour of the chosen beams. This element is thin, shear flexible, isometric quadrilateral shell with four nodes and five degree of freedom per node, utilizing reduced integration and bilinear interpolation scheme. Finite element models were developed using their centreline dimensions based on the nominal external dimensions. Keerthan and Mahendran [13] found that the effect of corners on the shear buckling behaviour of LSB is negligible (less than 1%). Therefore in the finite element models used here, the corner radius was not included. Finite element models were created using MD PATRAN R 2.1 pre-processing facilities and then submitted to ABAQUS for the analysis. The results were also viewed using MD PATRAN R 2.1 post-processing facilities. S4R5 shell elements were used with a suitable mesh size of 5mm x 5mm for the entire cross-section and length of steel beam sections. Eigenvalue buckling analysis is generally used to estimate the critical buckling loads of a steel structure. ABAQUS uses the subspace iteration Eigenslover in its buckling analyses. Eigenvalues, also known as load multipliers, are extracted in this analysis and the lowest values are important. The buckling modes are the most useful outcomes in the eigenvalue analysis, since they predict the likely failure mode of the member. In the analyses of this study, four buckling mode shapes were chosen.

In the elastic buckling analyses undertaken in this study the elastic modulus (E) and Poisson's ratio (ν) were taken as 200,000 MPa and 0.3, respectively. To provide simply supported conditions for the shear panels of LSB, LCB, RHFB, THFB and PG, the following boundary conditions were applied at the supports and the loading point (midspan).

- Simply supported in-plane - Both ends fixed against in-plane vertical deflection but unrestrained against in-plane rotation, and one end fixed against longitudinal horizontal displacement.

- ❖ Simply supported out-of-plane - Both ends fixed against out-of-plane horizontal deflection and twist rotation, but unrestrained against minor axis rotation.

Figure 3 shows the geometry and finite element mesh of hollow flange and open steel beams while Figure 4 shows the finite element models of LSB and plate girder (PG). The vertical translation was not restrained at the loading point. Table 1 shows the boundary conditions used along the edges of the model. Shear centre was located in the web for symmetrical steel beams such as RHCB, doubly symmetric THFB and PG. Therefore the load was applied through the web for these beams as shown in Figure 4 (a). Shear centre was located away from the web for monosymmetric steel beams such as LSB, LCB and monosymmetric THFB. Hence the applied loading was based on the shear flows and forces in LSB, LCB and monosymmetric THFB to eliminate any torsional loading effects (see Figure 4 (b)). The loading and boundary conditions in the finite element models used in this research are similar to those used by Keerthan and Mahendran [13] in their research on the shear buckling behaviour of LSBs.

LaBoube [2] and Hancock and Pham [5] used equal angle steel straps on both top and bottom flanges adjacent to the loading and reaction points to prevent section/flange distortion and lateral buckling at the loading and reaction points. Hence lateral restraints were applied to both top and bottom flanges at the loading and support points for open channel sections. Further details of the finite element models of cold-formed steel beams in shear can be found in Keerthan and Mahendran [13,14,17] and Keerthan et al. [18].

2.2. Elastic Shear Buckling Analyses

2.2.1. General

In this section the results from the elastic buckling analyses of all the open and hollow flange steel beams are presented and discussed. They included their shear buckling loads and modes, and in particular shear buckling coefficients.

Figures 5 (a) to (e) show the typical shear buckling modes of LCB, PG, RHFB, LSB and monosymmetric THFB, respectively. As seen in Figures 5 (c) to (e), shear buckling occurred within the clear height of web (between the two hollow flanges) for the sections with hollow

flanges. The sections with hollow flanges provide many structural advantages. There are no free edges and the sections have a low width to thickness (b/t) compared with other open cold-formed sections, which combine to reduce the tendency of the section to buckle locally. The hollow flanges also provide a higher torsional stiffness. Elastic shear buckling stress of a rectangular plate is given by Timoshenko and Gere [19] as follows.

$$\tau_{cr} = \frac{k_v \pi^2 E}{12\left(1-\nu^2\right)}\left(\frac{t_w}{d_1}\right)^2 \tag{5}$$

where

d_1, t_w = Clear height and thickness of web

k_v = Shear buckling coefficient (5.34)

The shear buckling coefficient (k_v) of a plate simply supported on all four edges varies from 5.34 for a very long plate to 9.34 for a square plate. For a web element with a large depth to thickness ratio, its shear capacity is governed by its elastic shear buckling stress. The elastic critical shear buckling stress can be computed using Equation 5 if the relevant elastic shear buckling coefficient (k_v) is known. In this research k_v was determined using Equation 5 based on the elastic buckling load/stress from FEA.

In the early days the web-flange juncture of cold-formed steel beams was assumed as simply supported due to lack of means to evaluate it in a rational manner [2] Recent research by Lee et al. [20] has shown that the boundary condition at the flange-web juncture in practical designs is much closer to fixity for plate girders (PG). They showed that the assumption that the web panel is simply supported at the web-flange juncture leads to a significant underestimation of the ultimate shear strength because of the underestimation of the elastic shear buckling strength of plate girders.

2.2.2. Elastic Shear Buckling Coefficients of LSBs and LCBs

Keerthan and Mahendran [13,14] proposed the following simple equations (Eqs. 6 and 7) based on their FEA results for the determination of elastic shear buckling coefficients of LSBs (k_{LSB}) and LCBs (k_{LCB}) in terms of the shear buckling coefficients of web plates with simple-simple (k_{ss}) and simple-fixed (k_{sf}) boundary conditions (Eqs. 8 and 9). The latter case refers to web panels that have fixed conditions at the web-flange juncture and simply supported along

the other two edges. In this section this approach was extended to other sections such as RHFB, HFB and PG.

$$k_{LCB} = k_{ss} + 0.23(k_{sf} - k_{ss}) \quad (6)$$

$$k_{LSB} = k_{ss} + 0.87(k_{sf} - k_{ss}) \quad (7)$$

$$k_{ss} = 4 + \frac{5.34}{(a/d_1)^2} \quad \text{for } \frac{a}{d_1} < 1 \quad (8a)$$

$$k_{ss} = 5.34 + \frac{4}{(a/d_1)^2} \quad \text{for } \frac{a}{d_1} \geq 1 \quad (8b)$$

$$k_{sf} = \frac{5.34}{(a/d_1)^2} + \frac{2.31}{(a/d_1)} - 3.44 + 8.39(a/d_1) \quad \text{for } \frac{a}{d_1} < 1 \quad (9a)$$

$$k_{sf} = 8.98 + \frac{5.61}{(a/d^1)^2} - \frac{1.99}{(a/d_1)^3} \quad \text{for } \frac{a}{d_1} \geq 1 \quad (9b)$$

where a = Shear span of web panel, d_1 = Clear web height and a/d_1 = Aspect ratio.

Tables 2 and 3 compare the shear buckling coefficients of LSBs and LCBs with k_{ss} and k_{sf} for an aspect ratio of 1.0. Equation 6 shows that the shear buckling coefficient of LCBs (k_{LCB}) is closer to k_{ss} (9.34) while Equation 7 shows that the shear buckling coefficient of LSBs (k_{LSB}) is closer to k_{sf} (12.60). Similar observations can also be made from Tables 2 and 3. Hence the realistic support condition of LCB at the web-flange juncture is considered to be closer to a simply supported condition while that of LSB at the web-flange juncture is considered to be closer to a fixed supported condition. The shear buckling deformed shapes from FEA confirm these observations in Figure 6.

2.2.3. Elastic Shear Buckling Coefficients of RHFB, THFB and PG

In this research finite element analyses were conducted to determine the shear buckling coefficients of THFB, RHFB and PG. In all the analyses, a flange width (b_f) to clear web height (d_1) ratio of more than 0.4 was used. This is because most of the available steel sections have a b_f/d_1 ratio greater than about 0.4. Table 4 compares the shear buckling coefficients (k_v) determined from the elastic buckling analyses of monosymmetric and doubly symmetric HFBs with triangular flanges for an aspect ratio of 1.0. The web and flange thicknesses were assumed to be the same for THFBs ($t_f/t_w = 1$) as they are cold-formed from a single steel strip. The reference buckling coefficients, k_{ss} and k_{sf}, were determined by using

Equations 8 and 9, respectively. Table 4 indicates that k_{THFB} is close to k_{sf} (12.60). Hence the realistic support condition of doubly symmetric and monosymmetric THFBs at the web-flange juncture is considered to be closer to a fixed supported condition. Since k_{HFB} is close to k_{sf} (12.60) with even a t_f/t_w ratio of 1, higher t_f/t_w ratios were not considered in the analyses of THFBs. Similar observation was also made for LSBs for which also a t_f/t_w ratio of 1 was used. Buckling analysis results show that boundary condition at the web-flange juncture of THFB is equivalent to about 90% fixity.

Table 5 compares the shear buckling coefficients (k_v) determined from the elastic buckling analyses of rectangular hollow flange beams (RHFB) with an aspect ratio of 1.0. Unlike for LCBs, LSBs and THFBs, the effect of t_f/t_w ratio was investigated for RHFB and PG since the flange and web thicknesses can be different for these sections. Three different flange width to clear web height (b_f/d_1) ratios of 0.46, 0.53 and 0.75 were also considered. Figure 7 shows that the elastic shear buckling coefficient of RHFB rapidly increases when the thickness ratio increases to 1.6. However, it did not increase much after it exceeded 1.6. Hence it can be concluded that t_f/t_w ratio should be increased to 1.6 in order to gain about 90% fixity level for RHFBs.

Tables 6 and 7 compare the shear buckling coefficients (k_v) determined from the elastic buckling analyses of plate girders with an aspect ratio of 1.0. Figure 8 shows that the elastic shear buckling coefficient of plate girders rapidly increases when the t_f/t_w ratio increases up to 2.0. However, it did not increase much after it exceeded 2.0. Hence it can be concluded that the t_f/t_w ratio should be increased to 2.0 in order to gain about 80% fixity level for plate girders as seen in Figure 8. Figure 8 (a) shows that the shear buckling coefficients of plate girders were similar to Lee et al.'s [20] findings when the flange width to clear height ratio (b_f/d_1) exceeded 0.4. However, they were slightly different to Lee et al.'s [20] values when the b_f/d_1 ratio was less than 0.4 (see Figure 8 (b)). In this study plate girders (PG) were also considered in FEA for comparison purposes.

Figures 6 (a) to (g) show the typical deformed cross-sections of buckled LCB, PG, LSB, THFB and RHFB. They can be compared with the deformation shapes of plates with simply supported and fixed edges shown in Figures 6 (a) and (g), respectively. This observation shows that the boundary condition at the web-flange juncture of LCBs is closer to a simply

supported condition while that of LSB, THFB, RHFB (t_f/t_w > 1.6) and plate girder (t_f/t_w>2) at the web-flange juncture is closer to a fixed supported condition.

Since the LSB, THFB and RHFB have two rigid hollow flanges, the boundary condition at the web-flange juncture is much closer to a fixed condition than in the conventional open cold-formed steel members and hot-rolled and welded I-sections. The shear buckling coefficients of LSB, THFB and RHFB are higher than that of other open cold-formed steel and I-section beams. When we consider the same height beam sections, LSB, THFB and RHFB have a lower clear height and a higher shear buckling coefficient than other conventional open cold-formed steel beams and hot-rolled I-section beams. Therefore their elastic shear buckling strengths will be higher than those of other conventional open cold-formed and hot-rolled steel beams (see Equation 5).

2.3. Simple Equation to Predict the Elastic Shear Buckling Coefficients

Based on the elastic buckling analysis results, the following simple equation (Equation 10) was developed for the determination of the elastic shear buckling coefficients of both hollow flange and open section beams. For this purpose the minimum shear buckling coefficients of LCB, LSB, THFB, RHFB and PG from FEA were used (see Tables 2 to 7). Shear buckling coefficient equations include the effect of flange thickness to web thickness ratio (t_f/t_w) for RHFBs and PGs. For LCBs, LSBs and THFBs, flange thickness is equal to web thickness (t_f/t_w = 1.0). Therefore the effect of t_f/t_w on the shear buckling coefficient was not considered for LCBs, LSBs and THFBs. The values of k_{ss} and k_{sf} for a given aspect ratio can be determined from Equations 8 and 9, respectively. Tables 2 to 7 show that clear height to thickness ratio (d_1/t_w) does not affect the shear buckling coefficient of steel beams.

$$k_v = k_{ss} + k_n(k_{sf} - k_{ss}) \tag{10}$$

where k_v = Shear buckling coefficient and k_{ss}, k_{sf} = Shear buckling coefficients of plates with simple-simple and simple-fixed boundary conditions. k_n can be obtained from Table 8.

In Equation 10, the coefficient k_n represents the fixity level at the web-flange juncture of open and hollow flange cold-formed steel beams, which depends on the geometry of cold-formed steel sections. Equations 10 and Table 8 results were developed based on detailed elastic

buckling analyses. Table 8 shows that the boundary condition at the web-flange juncture of LCBs is equivalent to 23% fixed condition while it shows that boundary condition at the flange-web juncture of LSBs is equivalent to 87% fixed condition. Since the level of fixity at the web-flange juncture of hollow flange and open steel beams is the same for the available steel beams, Equation 10 is applicable for all the aspect ratios. It can be used for any type of cold-formed steel beams by selecting a suitable k_n coefficient from Table 8.

3. Non Linear Finite Element Analyses

Keerthan and Mahendran [17,21] developed nonlinear finite element models to investigate the shear behaviour and strength of LSBs and LCBs. For this purpose, a finite element program, ABAQUS Version 6.7 [16], was used. Appropriate parameters were chosen for the geometry, mechanical properties, loading and support conditions. Finite element models of single LSBs and LCBs with shear centre loading and simply supported boundary conditions were used to simulate 25 shear tests of back to back LSBs and 15 shear tests of LCBs under three-point loading. The model geometry was based on the measured dimensions and yield stresses of tested LSBs and LCBs. Table 9 and 10 give the measured dimensions and yield stresses of test specimens of LSBs and LCBs, respectively. Figure 9 shows the shear failure modes of 200x75x15x1.50 LCB (aspect ratio =1.0) from FEA and tests. The local imperfection was taken as $d_1/150$ and $0.006d_1$ for all the LSBs and LCBs, respectively. The critical imperfection shape was introduced using the *IMPERFECTION option in ABAQUS while residual stresses were neglected in FEA as their effect on the shear capacity of LSBs and LCBs was less than 1%. Further details of the finite element model of LSBs and LCBs are reported in Keerthan and Mahendran [17,21], respectively.

It is important to validate the developed finite element models for non-linear analyses of LSBs and LCBs subjected to shear. Tables 9 and 10 compare the FEA and test shear capacity results of LSBs and LCBs, respectively. The mean and COV of the ratio of test to FEA ultimate shear capacities LSBs are 0.99 and 0.028 while the mean and COV of the ratio of test to FEA ultimate shear capacities LCBs are 1.01 and 0.055, respectively. This indicates that the developed finite element models are able to predict the ultimate shear capacities of LSBs and LCBs. A detailed parametric study was then undertaken based on the validated finite element model to develop an extensive shear strength data base in addition to 25 LSB and 15 LCB test and FEA results.

In Tables 11 and 12, test and FEA shear capacities of LSBs and LCBs were compared with the corresponding shear capacities predicted by the current design rules in AS/NZS 4600 [15]. This comparison clearly shows that the shear capacities predicted by AS/NZS 4600 [15] design rules are less than test and FEA shear capacities. AS/NZS 4600 [15] design rules are very conservative as they do not include the post-buckling strength observed in the shear tests and FEA and the increased shear buckling coefficient. Therefore new equations were proposed to predict the shear capacity of LSB and LCBs based on FEA and experimental results. Details of these equations, FEA, test and parametric study for LSBs and LCBs are given in Keerthan and Mahendran [17,21]. In the following sections this work was extended to include HFBs, RHFBs and PGs to develop general shear capacity equations for open and hollow flange section beams.

4. Proposed Design Equations for the Shear Capacity of Open and Hollow Flange Steel Beams

New shear strength equations are proposed for open and hollow flange steel beams based on the current design capacity equations in the AS/NZS 4600 [15]. The increased shear buckling coefficient given by Equation 10 (k_v) is included to allow for the additional fixity in the web-flange juncture instead of k_v assumed as 5.34 in AS/NZS 4600 [15]. Equations 11 to 13 present the relevant design equations when post-buckling strength is not included, where f_{yw} is the web yield stress and d_1/t_w is the ratio of clear web height to web thickness.

$$V_v = V_{yw} = 0.60 f_{yw} d_1 t_w \qquad \text{for} \qquad \frac{d_1}{t_w} \le \sqrt{\frac{Ek_v}{f_{yw}}} \qquad \text{(Shear yielding capacity)} \qquad (11)$$

$$V_v = V_i = 0.60 \frac{\sqrt{Ek_v f_{yw}}}{\left[\frac{d_1}{t_w}\right]} d_1 t_w \qquad \text{for} \quad \sqrt{\frac{Ek_v}{f_{yw}}} < \frac{d_1}{t_w} \le 1.508\sqrt{\frac{Ek_v}{f_{yw}}}$$

$$\text{(Inelastic shear buckling capacity)} \qquad (12)$$

$$V_v = V_{cr} = \frac{0.905 Ek_v}{\left(\frac{d_1}{t_w}\right)^2} d_1 t_w \qquad \text{for} \qquad \text{(Elastic shear buckling capacity)} \qquad (13)$$

Long span LCB, LSB, doubly symmetric THFB and RHFB are being used in practical applications and do not have transverse stiffeners. To simulate this practical application, the

infinity aspect ratio was also considered. For this aspect ratio, Figure 10 presents the new design curves based on Equations 11 to 13 in combination with the proposed shear buckling coefficient equation in this paper (Equation 10), and compares them with the AS/NZS 4600 [15] design equations. It shows that the ultimate shear capacities predicted by the current design rules in AS/NZS 4600 are conservative because AS/NZS 4600 design rules assume that the web panel is simply supported at the juncture between the flange and web elements and uses a smaller shear buckling coefficient (k_v) of 5.34. However in this study it was found that the realistic support condition at the web-flange juncture of LCB is 23% closer to a fixed support condition while it is 87% and 90% closer to a fixed support for LSB and both RHFB and THFB, respectively. Therefore the assumption used by AS/NZS 4600 [15] may result in very conservative shear design for open and hollow flange steel beams.

Keerthan and Mahendran [17] proposed improved design equations for the ultimate shear strength of LSBs based on both FEA and test results. Their design equations can also be used for other cold-formed steel sections such as LCBs, THFB and RHFB, provided suitable predictive equations are available for their elastic shear buckling coefficient and post-buckling strength. Presumably because of lack of experimental evidence on the shear capacity of plates without stiffeners, design codes do not include the post-buckling strength in shear, and the design shear stress in webs is therefore limited by the elastic buckling capacity [22]. Hancock and Pham [5] investigated the post-buckling strength of LCBs using experimental studies and confirmed that post-buckling shear strength is present in LCB and that it can be included in their design. Keerthan and Mahendran [14,21] also investigated the post-buckling strength of LCBs using experimental and numerical studies, and made the same observations. Hence Equations 14 to 16 are proposed for open and hollow flange steel beams in which the available post-buckling strength is also included. Here post-buckling strength is included in the inelastic and elastic buckling regions to replace Equations 12 and 13. A new post-buckling coefficient (p_n) is introduced in the proposed equations for this purpose. New design Equations (Eqs. 14 to 16) are based on Keerthan and Mahendran [17], who used a similar approach for LSBs.

$$V_v = V_{yw} \quad \text{for} \quad \frac{d_1}{t_w} \le \sqrt{\frac{Ek_v}{f_{yw}}} \quad \text{(Shear yielding)} \tag{14}$$

$$V_v = V_i + p_n\left(V_{yw} - V_i\right) \text{ for } \sqrt{\frac{Ek_v}{f_{yw}}} < \frac{d_1}{t_w} \le 1.508\sqrt{\frac{Ek_v}{f_{yw}}} \text{ (Inelastic shear buckling)} \tag{15}$$

$$V_v = V_{cr} + p_n\left(V_{yw} - V_{cr}\right) \quad \text{for} \quad \frac{d_1}{t_w} > 1.508\sqrt{\frac{Ek_v}{f_{yw}}} \quad \text{(Elastic shear buckling)} \qquad (16)$$

where

p_n = post-buckling coefficient = 0.25 for LSB, HFB, RHFB, PG and p_n = 0.2 for LCB

Keerthan and Mahendran [13,14] found that post-buckling coefficients (p_n) of LSBs and LCBs are 0.25 and 0.20, respectively based on their test and FEA results. They also found that the post-buckling coefficients (p_n) did not change much (0.20 vs 0.25) when the web-flange juncture fixity level varied from 23% (LCBs) to 87% (LSBs). Since the level of fixity at the web-flange juncture is about the same for LSBs (87%), THFBs (90%), RHFBs (90%) and PGs (80%), the same post-buckling coefficient (p_n) of 0.25 can be used for theses beams. The ultimate shear capacities of any open and hollow flange cold-formed steel beams can be calculated using the proposed shear capacity equations (Equations 14 to 16) if the relevant elastic shear buckling coefficient (k_v) and the post-buckling coefficient (p_n) are known.

Figures 11 and 12 show the plots of shear strength versus web slenderness ratio (d_1/t_w) for LCBs and RHFBs with an aspect ratio of 1.0 based on the proposed Equations 14 to 16. Figure 11 shows that significant post-buckling strength is available for slender LCBs while Figure 12 shows the presence of significant post-buckling strength for slender THFBs through both a higher elastic buckling coefficient and the introduction of p_n of 0.25. A suitable capacity reduction factor (ϕ) was calculated and reported in Keerthan and Mahendran [17] as 0.95 for LSBs and LCBs based on test and FEA results. This value is consistent with the current AISI S100 recommendations [7].

5. Direct Strength Method

The direct strength method provides simple design procedures to determine the ultimate capacities of cold-formed steel members. Proposed design equations (Eqs. 11 to 13 and 14 to 16) are therefore recast in the new direct strength method format as reported in Keerthan and Mahendran [17] and are given as Equations 17 to 19 and 21 to 23. These equations include the accurate shear buckling coefficient that takes into account the effects of web-flange fixity. Slenderness is calculated using Equation 20. Equations 17 to 19 present the proposed direct strength method (DSM) based design equations in which post-buckling strength is not included while Equation 21 and 23 include the available post-buckling strength.

(a) Shear capacity of cold-formed steel beams without post-buckling strength

$$\frac{V_v}{V_{yw}} = 1 \qquad \lambda \le 0.815 \tag{17}$$

$$\frac{V_v}{V_{yw}} = \frac{0.815}{\lambda} \qquad 0.815 < \lambda \le 1.23 \tag{18}$$

$$\frac{V_v}{V_{yw}} = \frac{1}{\lambda^2} \qquad \lambda > 1.23 \tag{19}$$

where

$$\lambda = \sqrt{\left(\frac{V_{yw}}{V_{cr}}\right)} = 0.815\left(\frac{d_1}{t_w}\right)\sqrt{\left(\frac{f_{yw}}{Ek_v}\right)} \tag{20}$$

(b) Shear capacity of cold-formed steel beams with post-buckling strength

$$\frac{V_v}{V_{yw}} = 1 \qquad \lambda \le 0.815 \tag{21}$$

$$\frac{V_v}{V_{yw}} = \frac{0.815}{\lambda} + p_n\left(1 - \frac{0.815}{\lambda}\right) \qquad 0.815 < \lambda \le 1.23 \tag{22}$$

$$\frac{V_v}{V_{yw}} = \frac{1}{\lambda^2} + p_n\left(1 - \frac{1}{\lambda^2}\right) \qquad \lambda > 1.23 \tag{23}$$

p_n = post-buckling coefficient, For LSB, HFB, RHFB, I-section, p_n = 0.25 and For LCB, p_n = 0.2.

New design equations are also proposed for the shear capacity of cold-formed steel beams in a similar way to those of the section moment capacity of beams subject to local buckling (Eqs. 24 and 25). Two regions based on shear yielding and elastic shear buckling, are considered in Equations 24 and 25 as for hot-rolled I-sections [23]. In these equations, a power coefficient of “n” is used instead of 0.4. It is proposed that it can be taken conservatively as 0.50 and 0.55 for LSBs and LCBs based on their test and FEA results reported in Keerthan and Mahendran [17,21]. They also found that the post-buckling coefficients (n) did not change much (0.50 vs 0.55) when the web-flange juncture fixity varied from 87% (LSBs) to 23% (LCBs). Since the level of fixity at the web-flange juncture is about the same for LSBs (87%), THFBs (90%), RHFBs (90%) and PG (80%) the same post-buckling coefficient (n) of 0.50 is recommended for LSBs, THFBs, RHFBs and PGs.

$$\frac{V_v}{V_y} = 1 \qquad \lambda \leq 0.815 \tag{24}$$

$$V_V = \left[1 - 0.15\left(\frac{V_{cr}}{V_y}\right)^n\right]\left(\frac{V_{cr}}{V_y}\right)^n V_y \quad \lambda > 0.815 \tag{25}$$

n = post-buckling coefficient = 0.50 for LSB, HFB, RHFB, I-section and *n* = 0.55 for LCBs

Figure 13 compares the shear design curves based on the proposed DSM based shear strength equations with FEA and available experimental results of LCBs, LSBs and plate girders (PG). This figure is in a non-dimensional format, ie. V_v/V_y versus $\lambda = (V_y/V_{cr})^{0.5}$. For comparison purposes, test results of plate girders (PG) from Lee et al. [20] are also included in this figure. Tables 11 to 13 show the FEA and test results of LSBs and LCBs and PGs, respectively, in the DSM format. Both experimental and numerical analyses show that there is considerable amount of post-buckling strength for LSBs, LCBs and PG subjected to shear, in particular for LSBs, LCBs and PG with large clear web height to thickness (d_1/t_w) ratios. Hence post-buckling shear strength can be taken into account in the design of LSBs and LCBs but also for other cold-formed steel beams including THFB and RHFB. It is clear from Figure 13 that the new shear strength equations (Eqs. 21 to 23; 24 and 25) that include post-buckling are able to predict the shear strengths of LSBs and LCBs more accurately using the proposed equations in this paper. The ultimate shear capacities of LCB, LSB, THFB and RHFB predicted by the current AS/NZS 4600 design rules are very conservative as the potential post-buckling strength has not been included while also assuming that web panels are simply supported at the web-flange juncture (Tables 11 to 13). Further experimental studies can be undertaken to improve the predictions by simply recalibrating the post buckling coefficients p_n or n.

7. Conclusions

This paper has presented the details of an investigation into the shear behaviour and strength of open and hollow flange steel beams. Numerical analyses were conducted to investigate the shear buckling behaviour of open (LCBs and PGs) and hollow flange (LSBs, THFBs and RHFBs) steel beams. It was found that the web-flange juncture in LSB, THFB, RHFB and plate girder (PG) has some fixity. A simple equation was therefore proposed for the higher elastic shear buckling coefficient of steel beams based on finite element analysis results, and

was included in the proposed ultimate shear capacity equations including those based on the direct strength method. The presence of post-buckling strength was also included in the proposed equations using a new post buckling coefficient and hence the proposed design equations were able to predict the ultimate shear capacities of open and hollow flange cold-formed steel beams accurately. The paper has proposed a generalised, improved shear design method that can be adopted for any type of cold-formed steel beam.

Acknowledgements

The authors would like to thank Australian Research Council for their financial support and the Queensland University of Technology for providing the necessary facilities and support to conduct this research project.

References

[1] OneSteel Australian Tube Mills (2008), (OATM), LiteSteel Beam Publication, Brisbane, Australia.

[2] LaBoube, R.A. and Yu, W.W. (1978), Cold-formed Steel Beam Webs Subjected Primarily to Shear, Research Report, American Iron and Steel Institute, University of Missouri-Rolla, Rolla, USA.

[3] Aswegan, K. and Moen, C. D. (2012), Critical Elastic Shear Buckling Stress Hand Solution for C- and Z-Sections Including Cross- Section Connectivity, Proceedings of the 21st International Specialty Conference on Cold-formed Steel Structures, St. Louis, Missouri, USA, pp 223-232.

[4] Pham, C.H. and Hancock, G.J. (2009), Shear Buckling of Thin-Walled Channel Sections, Journal of Constructional Steel Research, Vol 65, pp. 578-585.

[5] Pham, C.H. and Hancock, G.J. (2010), Experimental Investigation of High Strength C-Sections in Combined Bending and Shear, Journal of Structural Engineering, American Society of Civil Engineers, Vol. 136, pp. 866-878.

[6] Pham, C.H. and Hancock, G.J. (2012), Direct Strength Design of Cold-Formed C-Sections for Shear and Combined Actions, Journal of Structural Engineering, American Society of Civil Engineers, Vol. 138, pp. 759–768.

[7] American Iron and Steel Institute (AISI) (2012), North American Specification for the Design of Cold-formed Steel Structural Members, AISI, Washington, DC, USA.

[8] Anapayan, T., Mahendran, M. and Mahaarachchi, D. (2011), Section Moment Capacity Tests of LiteSteel Beams. Thin-Walled Structures, Vol. 49, pp. 502-512.

[9] Anapayan, T. and Mahendran, M. (2012), Improved Design Rules for Hollow Flange Sections Subject to Lateral Distortional Buckling. Thin-Walled Structures, Vol. 50, pp. 128-140.

[10] Keerthan, P. and Mahendran, M. (2010), Experimental Studies on the Shear Behaviour and Strength of LiteSteel Beams, Engineering Structures, Vol 32, pp. 3235-3247.

[11] Keerthan, P. and Mahendran (2013), Experimental Studies of the Shear Behavior and Strength of LiteSteel Beams with Stiffened Web Openings, Engineering Structures, Vol. 49, pp. 840-854.

[12] Keerthan, P. and Mahendran, M. (2008), Shear Behaviour of LiteSteel Beams, Proceedings of the $5t^h$ International Conference on Thin-Walled Structures, Brisbane, Australia, pp.411-418.

[13] Keerthan, P. and Mahendran, M. (2010), Elastic Shear Buckling Characteristics of LiteSteel Beams, Journal of Constructional Steel Research, Vol 66, pp. 1309-1319.

[14] Keerthan, P. and Mahendran, M. (2013), Shear Buckling Characteristics of Cold-formed Steel Channel Beams, International Journal of Steel Structures, Vol.13, No.3, pp.385-399.

[15] Standards Australia/Standards New Zealand (SA) (2005), Australia/New Zealand Standard AS/NZS4600 Cold-Formed Steel Structures, Sydney, Australia.

[16] Hibbitt, Karlsson and Sorensen, Inc. (HKS) (2007), ABAQUS User's Manual, Inc., New York, USA.

[17] Keerthan, P. and Mahendran, M. (2011), New Design Rules for the Shear Strength of LiteSteel Beams, Journal of Constructional Steel Research Vol 67, pp. 1050-1063.

[18] Keerthan, P., Mahendran, M. and Hughes, D. (2014), Numerical Studies and Design of Hollow Flange Channel Beams Subject to Combined Bending and Shear Actions. Engineering Structures, 75, pp. 197-212.

[19] Timoshenko, S. P. and Gere, J.M. (1961), Theory of Elastic Stability, McGraw- Hill Book Co. Inc, New York.

[20] Lee, S.C., Davidson, J.S. and Yoo, C. (1996), Shear Buckling Coefficients of Plate Girder Web Panels, Journal of Computers and Structures, Vol. 59, pp. 789-795.

[21] Keerthan, P. and Mahendran, M. (2014), Numerical Modelling and Design of Lipped Channel Beams Subject to Shear, Proc. of the 7th European Conference on Steel and Composite Structures, Napoli, Italy, pp.445-446.

[22] Suter, G.T. and Humar, J.L. (1986), Post-Buckling Shear Strength of a Cold-formed Steel Joist, Proc. of the 5th International Specialty Conference on Cold-formed Steel Structures, St. Louis, Missouri, USA, pp. 225-237.

[23] Standards Australia/Standards New Zealand (SA) (1998). Australian/New Zealand Standard AS/NZS 4100 Steel Structures, Sydney, Australia.

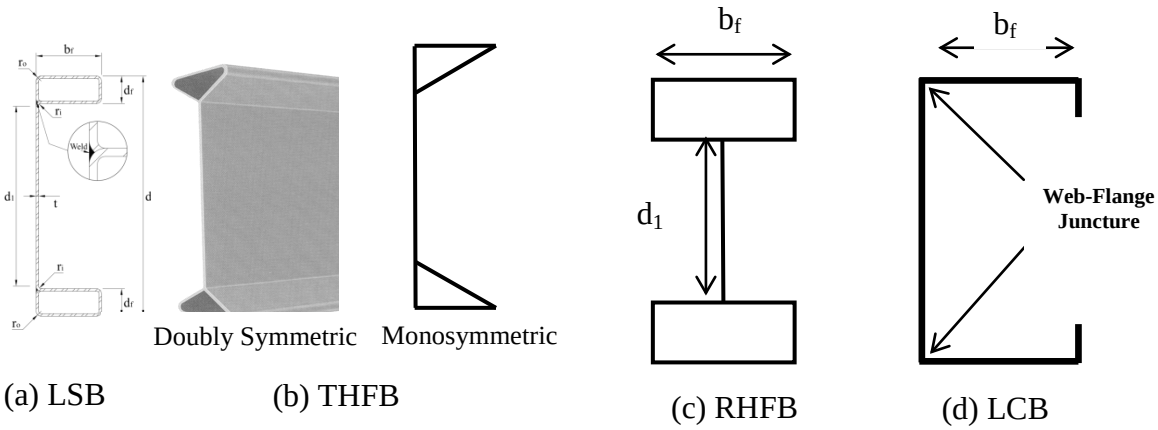

(a) LSB (b) THFB (c) RHFB (d) LCB

Figure 1: Hollow Flange and Open Cold-formed Steel Beams

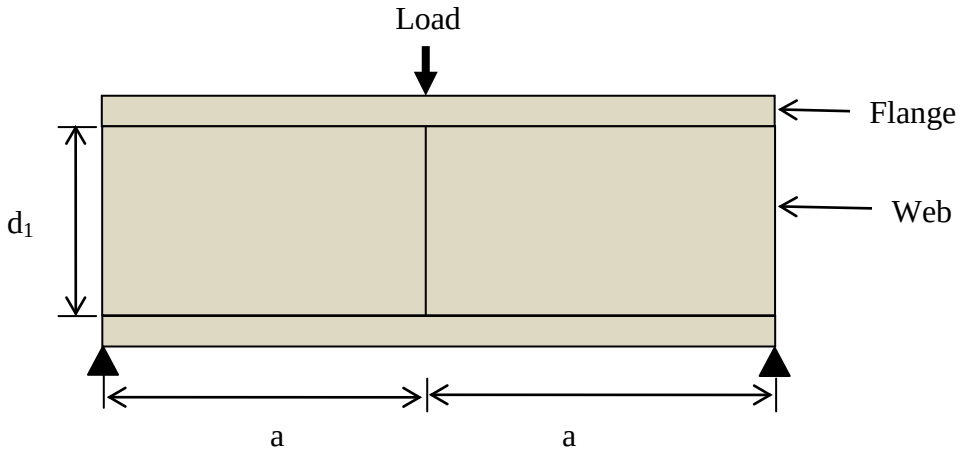

Note: d_1 is Clear height of web

Figure 2: Schematic Diagram of Shear Loading Set-up

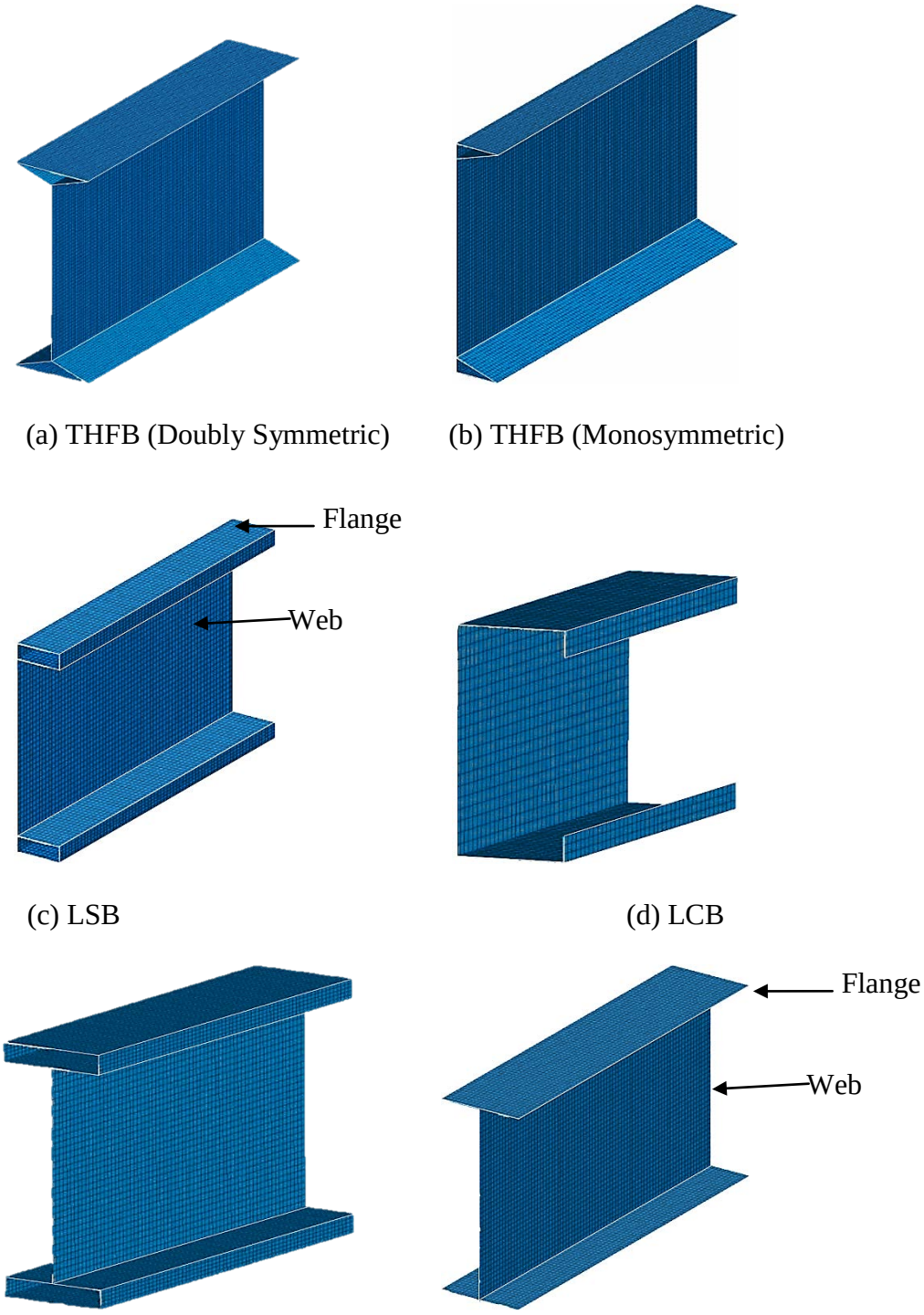

(a) THFB (Doubly Symmetric) (b) THFB (Monosymmetric)

(c) LSB (d) LCB

(e) RHFB (f) Plate Girder

Figure 3: Geometry and Finite Element Mesh of Steel Beams

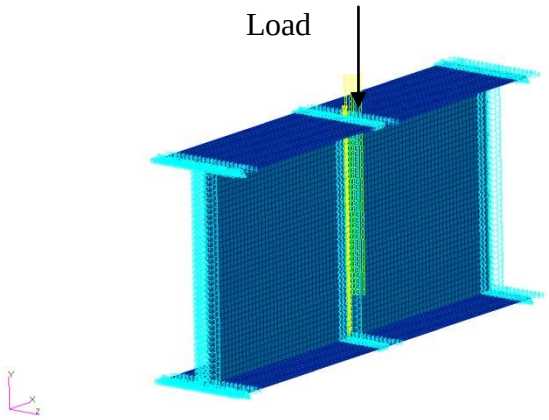

(a) Plate Girder (PG)

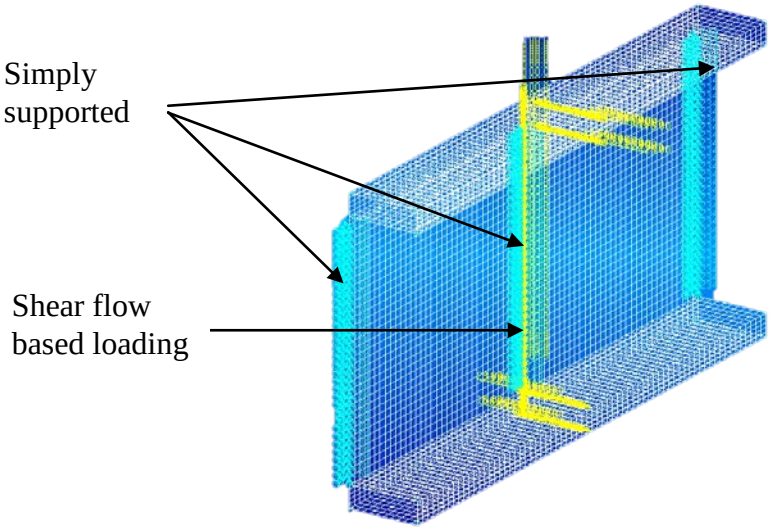

(b) LiteSteel Beam (LSB)

Figure 4: Ideal Finite Element Models of Steel Beams

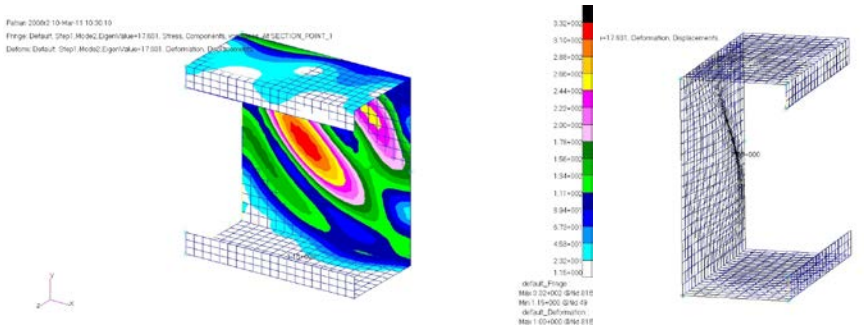

(a) Lipped Channel Beam (LCB)

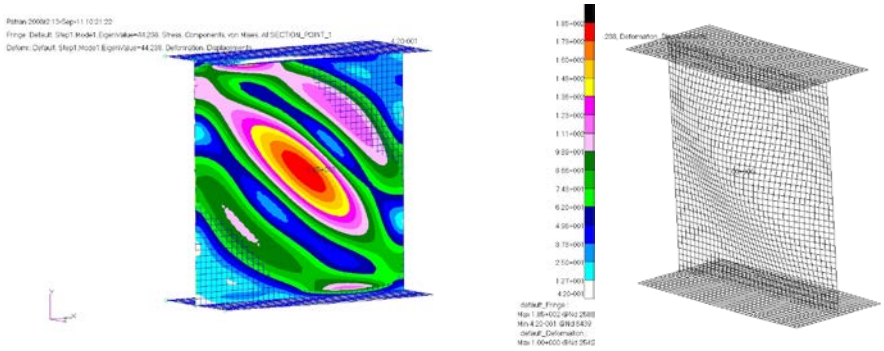

(b) Plate Girder (PG)

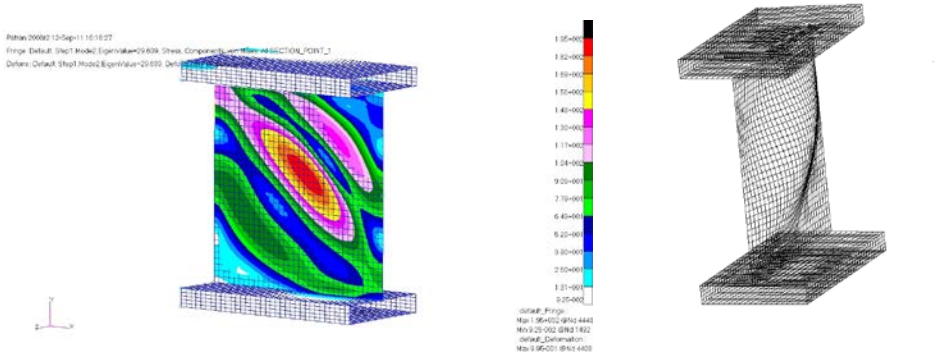

(c) Rectangular Hollow Flange Beam (RHFB)

Figure 5: Shear Buckling Modes of Steel Beams (Aspect Ratio = 1.0)

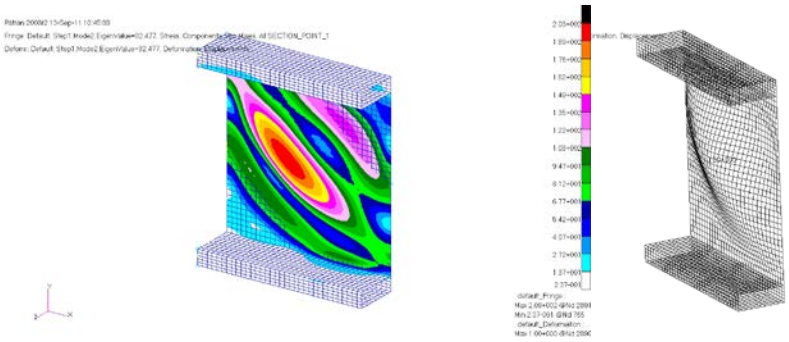

(d) LiteSteel Beam (LSB)

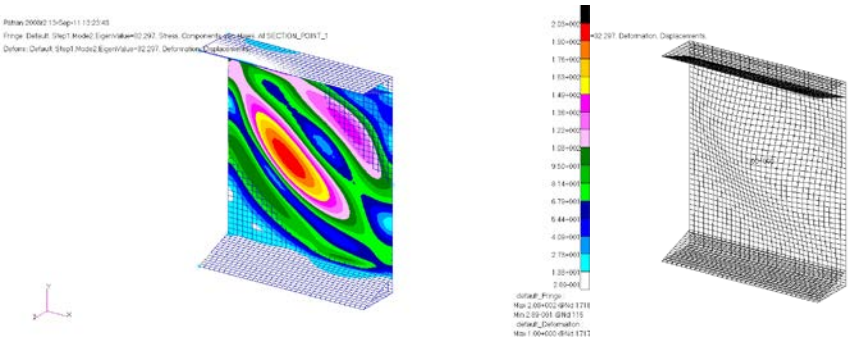

(e) Monosymmetric Triangular Hollow Flange Beam (THFB)

Figure 5: Shear Buckling Modes of Steel Beams (Aspect Ratio = 1.0)

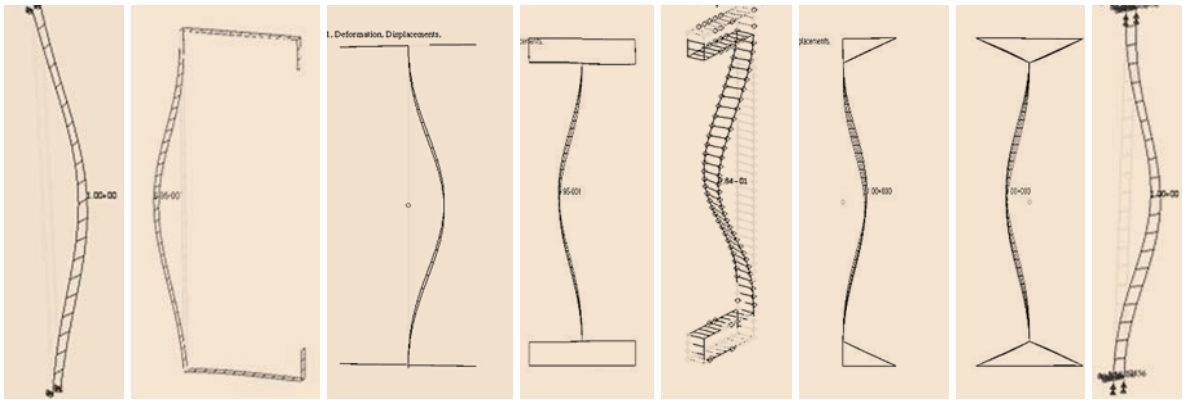

(a) Simple Supports (b) LCB (c) PG (d) RHFB (e) LSB (f) THFB (g) Fixed Supports

Figure 6: Shear Buckling Deformed Shapes

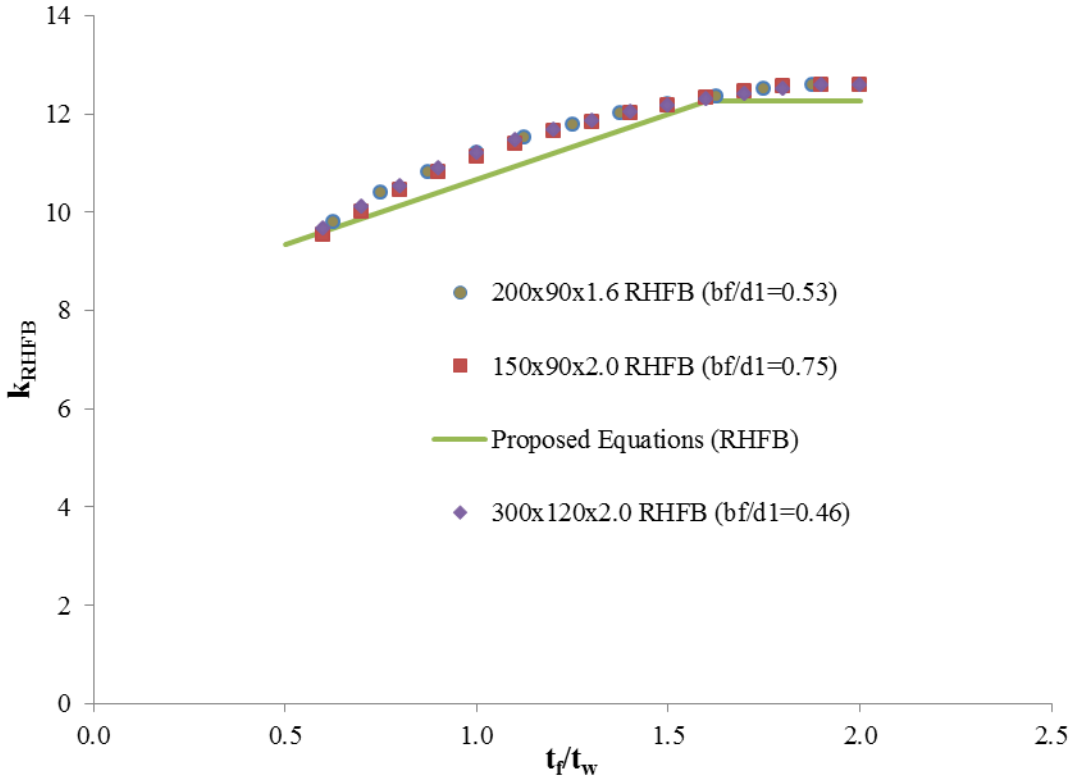

Figure 7: Shear Buckling Coefficients of Rectangular Hollow Flange Beams (RHFB)

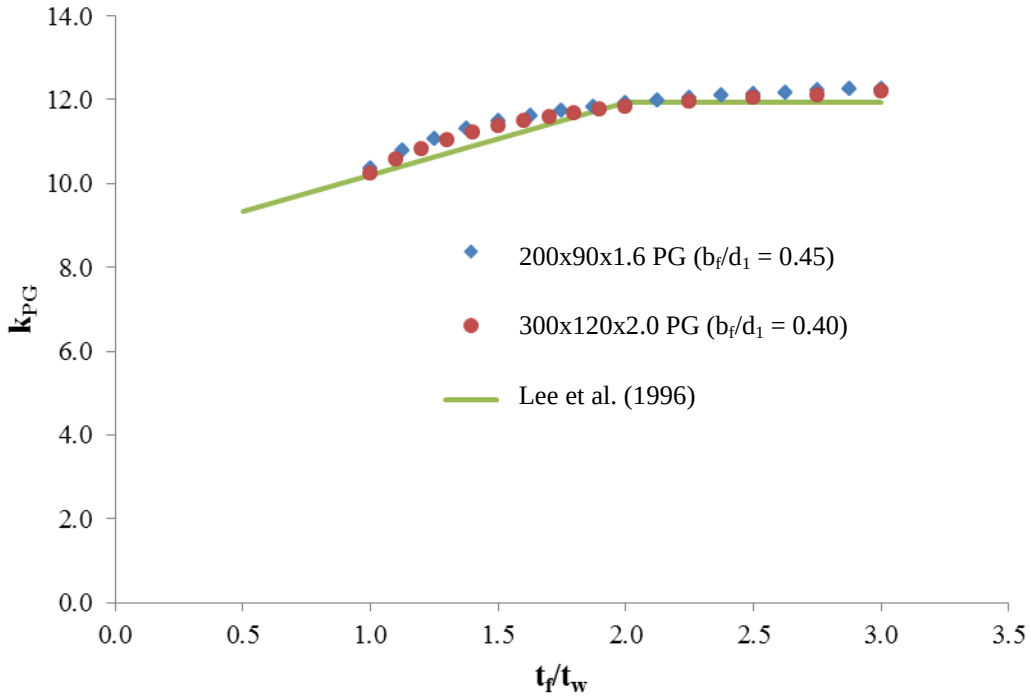

(a) Flange width to clear height ratio (b_f/d_1) = 0.40 and 0.45

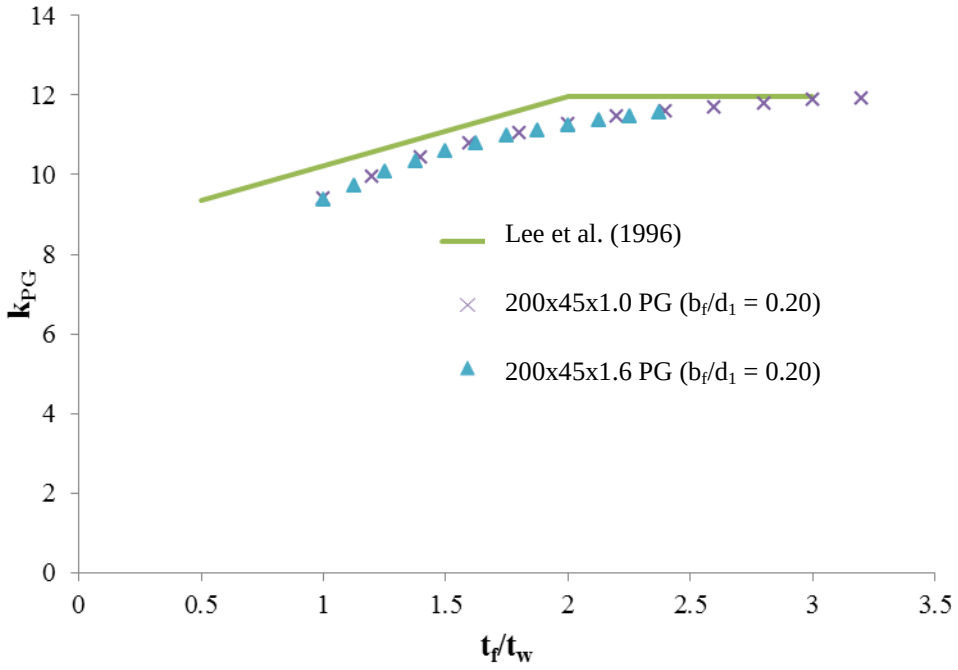

(b) Flange width to clear height ratio (b_f/d_1) = 0.20

Figure 8: Shear Buckling Coefficients of Plate Girders

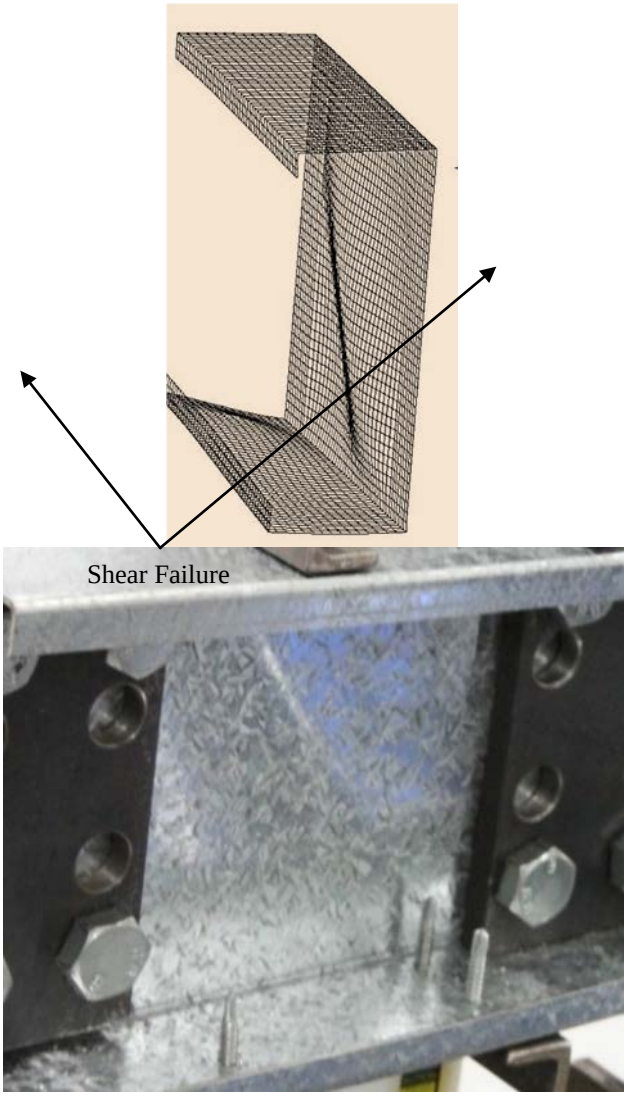

(a) FEA (b) Experiment

Figure 9: Failure mode of 200x75x15x1.50 LCB (Aspect ratio =1.0)

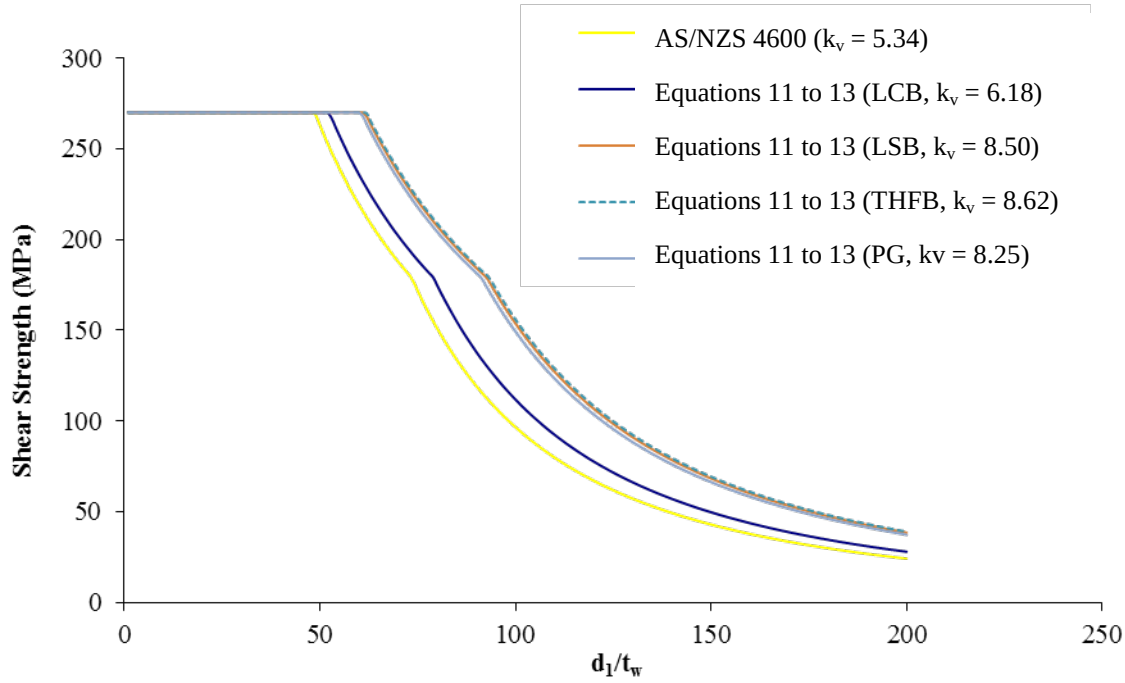

Figure 10: Shear Strength versus Clear Web Height to Thickness Ratio (d_1/t_w) for Long Span Beams (f_{yw} = 450 MPa).

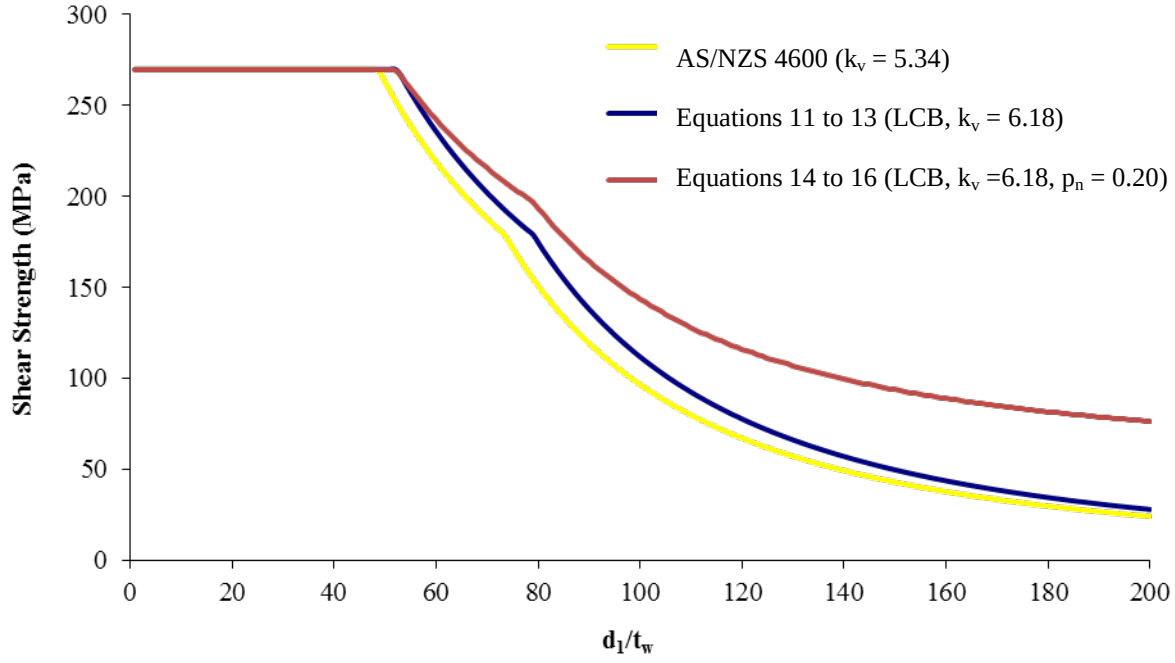

Figure 11: Shear Strength versus Clear Web Height to Thickness Ratio (d_1/t_w) for Long Span LCBs (f_{yw} = 450 MPa)

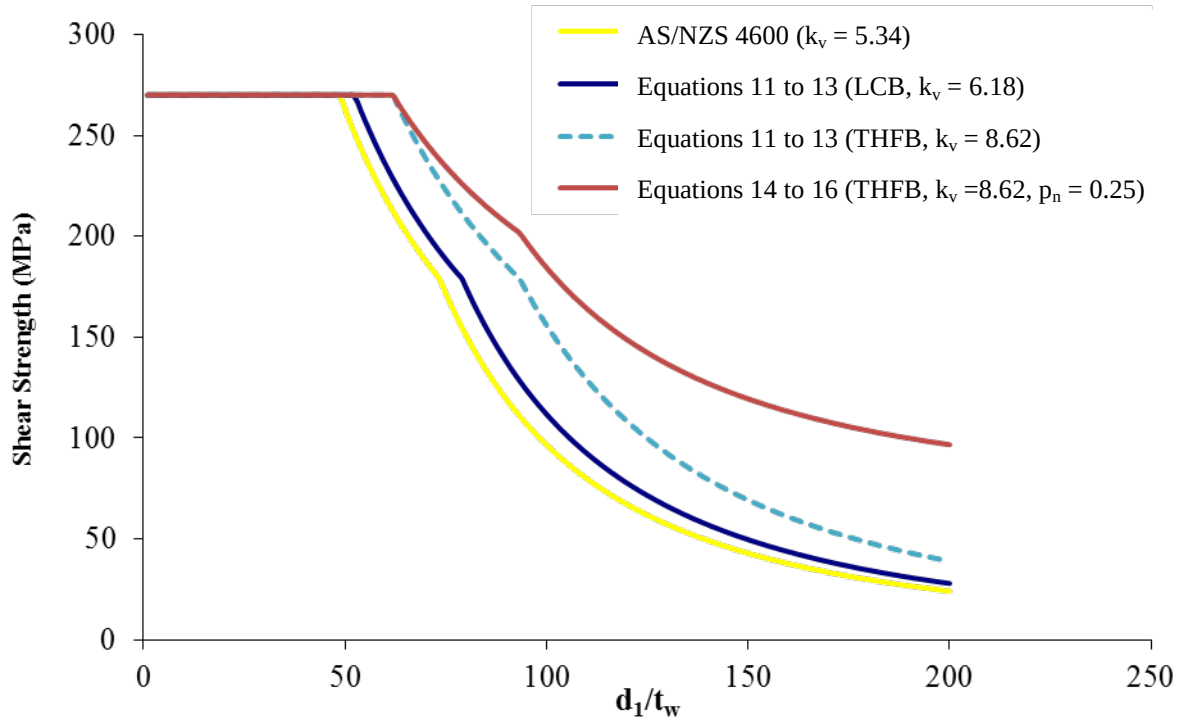

Figure 12: Shear Strength versus Clear Web Height to Thickness Ratio (d_1/t_w) for Long Span THFBs (f_{yw} = 450 MPa)

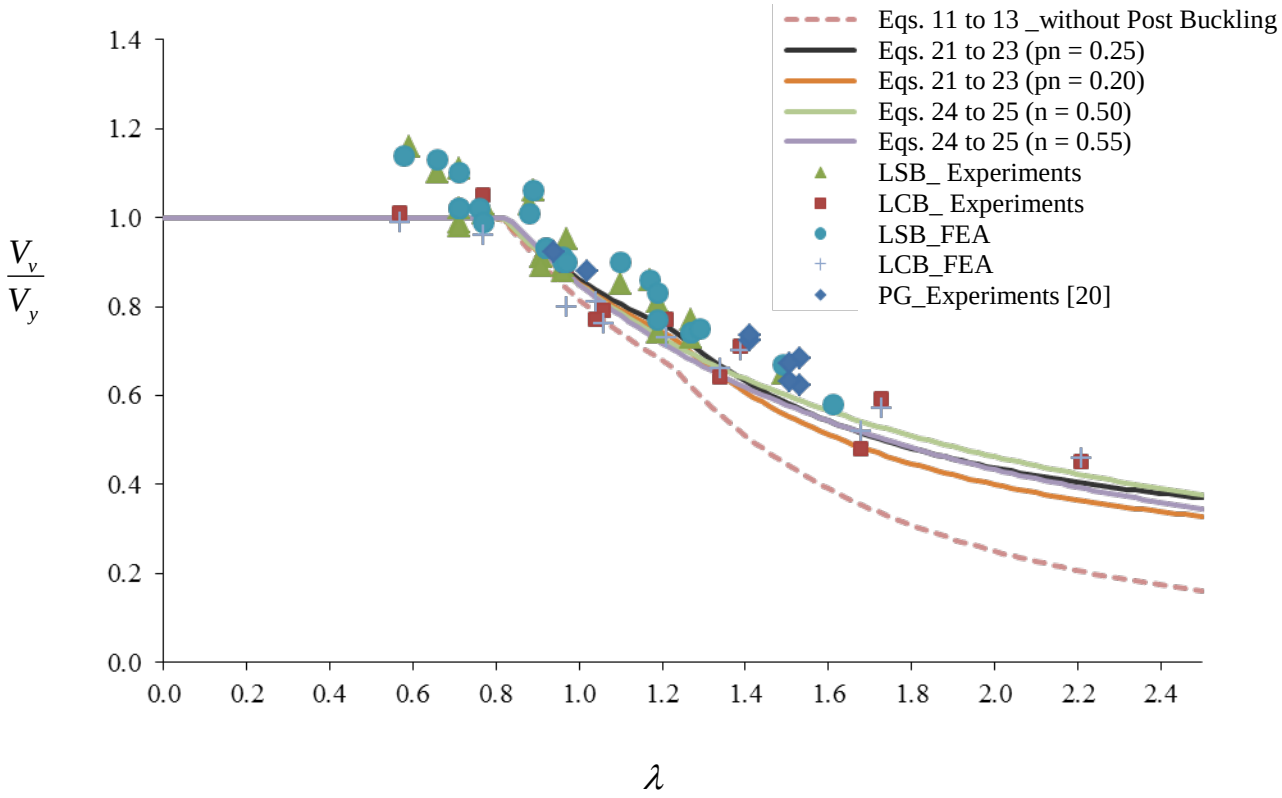

Figure 13: Comparison of Shear Capacities of LSBs, LCBs and PGs with DSM Based Design Equations

Table 1: Boundary Conditions Used in the Finite Element Model of Steel Beams

Edges	u	v	w	θ_x	θ_y	θ_z
Left and Right (Support)	0	1	1	1	0	0
Middle (Loading Point)	1	0	1	1	0	0

Note: u, v and w are translations while θ_x, θ_y and θ_z are rotations in the x, y and z directions, respectively. 0 denotes free and 1 denotes restrained.

Table 2: Comparison of Shear Buckling Coefficients of LSBs

LSB Section $dxb_fxd_fxt_w$	b_f/d_1	k_{ss}	k_{sf}	k_{LSB}
125x45x15x1.6	0.47	9.34	12.60	12.58
125x45x15x2.0	0.47	9.34	12.60	12.59
150x45x15x1.6	0.38	9.34	12.60	12.57
150x45x15x2.0	0.38	9.34	12.60	12.58
200x45x15x1.6	0.26	9.34	12.60	12.19
200x60x20x2.0	0.28	9.34	12.60	12.57
200x60x20x2.5	0.28	9.34	12.60	12.58
250x60x20x2.0	0.29	9.34	12.60	12. 45
250x75x25x2.5	0.38	9.34	12.60	12.58
250x75x25x3.0	0.38	9.34	12.60	12.59
300x60x20x2.0	0.23	9.34	12.60	12.41
300x75x25x2.5	0.30	9.34	12.60	12.43
300x75x25x3.0	0.30	9.34	12.60	12.45

Note: d = depth, b_f = flange width, t_w = web thickness, d_f = flange height = $b_f/3$, flange thickness $t_f = t_w$

Table 3: Comparison of Shear Buckling Coefficients of LCBs

LCB Section $dxb_fxb_lxt_w$	b_f/d_1	k_{ss}	k_{sf}	k_{LCB}	Web-Flange Fixity Level
64x38x13.0x2.5	0.59	9.34	12.60	10.50	36%
100x80x20x1.0	0.80	9.34	12.60	10.72	42%
102x51x12.5x1.0	0.50	9.34	12.60	10.43	34%
102x51x12.5x1.2	0.50	9.34	12.60	10.43	34%
102x51x12.5x1.5	0.50	9.34	12.60	10.43	34%
102x51x12.5x1.9	0.50	9.34	12.60	10.43	34%
152x64x14.5x1.0	0.42	9.34	12.60	10.25	28%
152x64x14.5x1.2	0.42	9.34	12.60	10.25	28%
152x64x14.5x1.5	0.42	9.34	12.60	10.25	28%
152x64x14.5x1.9	0.42	9.34	12.60	10.25	28%
152x64x14.5x2.4	0.42	9.34	12.60	10.26	28%
203x76x16.0x1.5	0.37	9.34	12.60	10.18	26%
203x76x16.0x1.9	0.37	9.34	12.60	10.18	26%
203x76x16.0x2.4	0.37	9.34	12.60	10.18	26%
254x76x19.0x1.9	0.30	9.34	12.60	10.11	24%
254x76x19.0x2.4	0.30	9.34	12.60	10.11	24%
300x96x28.0x2.4	0.32	9.34	12.60	10.12	24%
300x96x28.0x3.0	0.32	9.34	12.60	10.12	24%
350x125x30x3.0	0.36	9.34	12.60	10.14	25%
500x150x30x2.0	0.30	9.34	12.60	10.08	23%

Note: d = depth, b_f = flange width , b_l= lip width, t_w = web thickness, flange thickness $t_f = t_w$

Table 4: Comparison of Shear Buckling Coefficients of THFBs

No.	THFB Section $dxb_fxd_fxt_w$	Type	b_f/d_1	k_{sf}	k_{THFB}
1	150x90x15x1.6	Symmetric	0.75	12.60	12.58
2	150x90x15x2.0	Symmetric	0.75	12.60	12.58
3	200x90x15x1.6	Symmetric	0.53	12.60	12.30
4	300x120x20x2.0	Symmetric	0.46	12.60	12.53
5	300x120x20x2.5	Symmetric	0.46	12.60	12.49
6	300x120x20x3.0	Symmetric	0.46	12.60	12.45
7	150x45x15x1.6	Monosymmetric	0.38	12.60	12.57
8	150x45x15x2.0	Monosymmetric	0.38	12.60	12.58
9	200x45x15x1.6	Monosymmetric	0.26	12.60	12.22
10	200x45x15x2.0	Monosymmetric	0.26	12.60	12.23

Note: d = depth, d_f = depth of flange, b_f = flange width, t_w = web thickness, flange thickness $t_f = t_w$

Table 5: Comparison of Shear Buckling Coefficients of RHFBs (b_f/d_1 = 0.46, 0.53 and 0.75 and Aspect ratio 1.0)

No.	Section $dxb_fxd_fxt_wxt_f$	t_f/t_w	b_f/d_1	k_{RHFB}
1	200x90x15x1.6x1.0	0.63	0.53	9.80
2	200x90x15x1.6x1.2	0.75	0.53	10.41
3	200x90x15x1.6x1.4	0.88	0.53	10.82
4	200x90x15x1.6x1.6	1.00	0.53	11.21
5	200x90x15x1.6x1.8	1.13	0.53	11.53
6	200x90x15x1.6x2.0	1.25	0.53	11.79
7	200x90x15x1.6x2.2	1.38	0.53	12.01
8	200x90x15x1.6x2.4	1.50	0.53	12.19
9	200x90x15x1.6x2.6	1.63	0.53	12.36
10	200x90x15x1.6x2.8	1.75	0.53	12.51
11	200x90x15x1.6x3.0	1.88	0.53	12.58
12	200x90x15x1.6x3.2	2.00	0.53	12.59
13	150x90x15x2.0x1.2	0.60	0.75	9.55
14	150x90x15x2.0x1.4	0.70	0.75	10.02
15	150x90x15x2.0x1.6	0.80	0.75	10.44
16	150x90x15x2.0x1.8	0.90	0.75	10.81
17	150x90x15x2.0x2.0	1.00	0.75	11.13
18	150x90x15x2.0x2.2	1.10	0.75	11.40
19	150x90x15x2.0x2.4	1.20	0.75	11.64
20	150x90x15x2.0x2.6	1.30	0.75	11.84
21	150x90x15x2.0x2.8	1.40	0.75	12.02
22	150x90x15x2.0x3.0	1.50	0.75	12.18
23	150x90x15x2.0x3.2	1.60	0.75	12.33
24	150x90x15x2.0x3.4	1.70	0.75	12.47
25	150x90x15x2.0x3.6	1.80	0.75	12.57
26	150x90x15x2.0x3.8	1.90	0.75	12.58
27	150x90x15x2.0x4.0	2.00	0.75	12.59
28	300x120x20x2.0x1.2	0.60	0.46	9.66
29	300x120x20x2.0x1.4	0.70	0.46	10.12
30	300x120x20x2.0x1.6	0.80	0.46	10.53
31	300x120x20x2.0x1.8	0.90	0.46	10.89
32	300x120x20x2.0x2.0	1.00	0.46	11.20
33	300x120x20x2.0x2.2	1.10	0.46	11.47
34	300x120x20x2.0x2.4	1.20	0.46	11.67
35	300x120x20x2.0x2.6	1.30	0.46	11.87
36	300x120x20x2.0x2.8	1.40	0.46	12.03
37	300x120x20x2.0x3.0	1.50	0.46	12.17
38	300x120x20x2.0x3.2	1.60	0.46	12.30
39	300x120x20x2.0x3.4	1.70	0.46	12.42
40	300x120x20x2.0x3.6	1.80	0.46	12.52
41	300x120x20x2.0x3.8	1.90	0.46	12.58
42	300x120x20x2.0x4.0	2.00	0.46	12.59

Note: d = depth, d_f = depth of flange, b_f = flange width, t_w = web thickness, t_f = flange thickness

Table 6: Comparison of Shear Buckling Coefficients of Plate Girders (b_f/d_1 = 0.40 and 0.45 and Aspect Ratio = 1.0)

No.	Section $dxb_fxt_wxt_f$	t_f/t_w	b_f/d_1	k_{PG}
1	200x90x1.6x1.6	1.00	0.45	10.36
2	200x90x1.6x1.8	1.13	0.45	10.78
3	200x90x1.6x2.0	1.25	0.45	11.08
4	200x90x1.6x2.2	1.38	0.45	11.31
5	200x90x1.6x2.4	1.50	0.45	11.49
6	200x90x1.6x2.6	1.63	0.45	11.63
7	200x90x1.6x2.8	1.75	0.45	11.75
8	200x90x1.6x3.0	1.88	0.45	11.84
9	200x90x1.6x3.2	2.00	0.45	11.92
10	200x90x1.6x3.4	2.13	0.45	11.99
11	200x90x1.6x3.6	2.25	0.45	12.05
12	200x90x1.6x3.8	2.38	0.45	12.10
13	200x90x1.6x4.0	2.50	0.45	12.14
14	200x90x1.6x4.2	2.63	0.45	12.18
15	200x90x1.6x4.4	2.75	0.45	12.22
16	200x90x1.6x4.6	2.88	0.45	12.25
17	200x90x1.6x4.8	3.00	0.45	12.27
18	300x120x2x2.0	1.00	0.40	10.24
19	300x120x2x2.2	1.10	0.40	10.57
20	300x120x2x2.4	1.20	0.40	10.83
21	300x120x2x2.6	1.30	0.40	11.04
22	300x120x2x2.8	1.40	0.40	11.22
23	300x120x2x3.0	1.50	0.40	11.36
24	300x120x2x3.2	1.60	0.40	11.49
25	300x120x2x3.4	1.70	0.40	11.59
26	300x120x2x3.6	1.80	0.40	11.68
27	300x120x2x3.8	1.90	0.40	11.76
28	300x120x2x4.0	2.00	0.40	11.82
29	300x120x2x4.0	2.25	0.40	11.96
30	300x120x2x5.0	2.50	0.40	12.05
31	300x120x2x4.0	2.75	0.40	12.12
32	300x120x2x6.0	3.00	0.40	12.19

Note: d = depth, b_f = flange width, t_w = web thickness and t_f = flange thickness

Table 7: Comparison of Shear Buckling Coefficients of Plate Girders

(b_f/d_1 = 0.20 and Aspect Ratio = 1.0)

No.	Section $dxb_fxt_wxt_f$	t_f/t_w	k_{PG}
1	200x40x1.0x1.0	1.00	9.39
2	200x40x1.0x1.2	1.20	9.96
3	200x40x1.0x1.4	1.40	10.43
4	200x40x1.0x1.6	1.60	10.78
5	200x40x1.0x1.8	1.80	11.06
6	200x40x1.0x2.0	2.00	11.28
7	200x40x1.0x2.2	2.20	11.45
8	200x40x1.0x2.4	2.40	11.58
9	200x40x1.0x2.6	2.60	11.70
10	200x40x1.0x2.8	2.80	11.79
11	200x40x1.0x3.0	3.00	11.87
12	200x40x1.0x3.2	3.20	11.93
13	200x40x1.6x1.6	1.00	9.37
14	200x40x1.6x1.8	1.13	9.74
15	200x40x1.6x2.0	1.25	10.07
16	200x40x1.6x2.2	1.38	10.35
17	200x40x1.6x2.4	1.50	10.59
18	200x40x1.6x2.6	1.63	10.80
19	200x40x1.6x2.8	1.75	10.97
20	200x40x1.6x3.0	1.88	11.12
21	200x40x1.6x3.2	2.00	11.25
22	200x40x1.6x3.4	2.13	11.36
23	200x40x1.6x3.6	2.25	11.46

Note: d = depth, b_f = flange width, t_w = web thickness and t_f = flange thickness

Table 8: Coefficient k_n for Open and Hollow Flange Steel Beams

Section	k_n	
Lipped Channel beam (LCB)	0.23	$\frac{b_f}{d_1} > 0.3$
Plate Girder (PG)	$0.8\left(1-\frac{2}{3}(2-\frac{t_f}{t_w})\right)$	$0.5 < \frac{t_f}{t_w} < 2.0$ $\quad \frac{b_f}{d_1} > 0.4$
	0.80	$\frac{t_f}{t_w} \geq 2.0$ $\quad \frac{b_f}{d_1} > 0.4$
Rectangular Hollow Flange Beam (RHFB)	$\left(0.82\frac{t_f}{t_w} - 0.41\right)$	$0.5 < \frac{t_f}{t_w} < 1.6$ $\quad \frac{b_f}{d_1} > 0.4$
	0.90	$\frac{t_f}{t_w} \geq 1.6$ $\quad \frac{b_f}{d_1} > 0.4$
LiteSteel Beam (LSB)	0.87	$\frac{b_f}{d_1} > 0.3$
Triangular Hollow Flange Beam (THFB) (Doubly Symmetric and MonoSymmetric)	0.90	$\frac{b_f}{d_1} > 0.3$

Note: b_f = flange width, d_1 = flat portion of clear height of web, t_w = web thickness and t_f = flange thickness

Table 9: Comparison of Ultimate Shear Capacities of LSBs from FEA and Tests

LSB Sections $dxb_fxd_fxt_w$	d_1 (mm)	t_w (mm)	f_{yw} (MPa)	a/d_1	Ultimate Shear Capacities (kN)		Test/FEA
					Test	FEA	
150x45x15x2.0	120.0	1.97	437.1	1.0	68.5	70.0	0.98
200x45x15x1.6	169.6	1.61	452.1	1.0	63.6	63.5	1.00
200x60x20x2.0	160.0	1.97	440.4	1.0	88.2	88.5	1.00
200x60x20x2.5	161.0	2.50	443.3	1.0	119.3	118.0	1.01
250x60x20x2.0	209.6	1.96	451.9	1.0	90.1	93.0	0.97
250x75x25x2.5	201.0	2.51	446.0	1.0	139.6	136.5	1.02
300x60x20x2.0	262.3	1.97	459.7	1.0	93.0	96.0	0.97
300x75x25x2.5	250.0	2.51	449.1	1.0	143.7	151.5	0.95
125x45x15x2.0	95.2	1.94	444.4	1.5	56.9	56.0	1.02
150x45x15x1.6	120.0	1.58	454.2	1.5	45.8	47.8	0.96
150x45x15x1.6	120.0	1.58	454.2	1.5	47.1	47.8	0.99
150x45x15x1.6	120.0	1.58	454.2	1.5	47.0	47.8	0.98
150x45x15x2.0	120.0	1.97	422.6	1.5	61.1	61.0	1.00
150x45x15x2.0	120.0	1.97	422.6	1.5	58.8	61.0	0.96
150x45x15x2.0	120.0	1.97	422.6	1.5	59.5	61.0	0.98
200x60x20x1.6	169.6	1.61	452.1	1.5	56.8	55.0	1.03
200x45x15x1.6	169.6	1.61	452.1	1.5	54.2	55.0	0.99
200x60x20x2.0	160.0	1.97	440.4	1.5	74.0	76.0	0.97
200x60x20x2.5	161.0	2.50	443.3	1.5	110.0	109.0	1.01
250x60x20x2.0	209.6	1.96	451.9	1.5	>75.0	83.0	NA
250x75x25x2.5	201.0	2.51	446.0	1.5	118.9	121.0	0.98
300x60x20x2.0	262.3	1.97	459.7	1.5	> 75.0	82.0	NA
300x75x25x2.5	250.0	2.51	449.1	1.5	125.1	131.0	0.95
200x60x20x2.0	160.0	1.97	440.4	1.6	79.4	75.0	1.06
200x60x20x2.5	161.0	2.50	443.3	1.6	107.9	106.0	1.02
Mean							0.99
COV							0.028

Note: d_1 = flat portion of clear height of web, f_{yw} = web yield stress, t_w = web thickness, a = shear span, and a/d_1 = aspect ratio.

Table 10: Comparison of Ultimate Shear Capacities of LCBs from FEA and Tests

LCB Sections $dxb_fxb_lxt_w$	d_1 (mm)	t_w (mm)	f_{yw} (MPa)	a/d_1	Ultimate Shear Capacities (kN)		Test/FEA
					Test	FEA	
200x75x15x1.9	197.0	1.92	515	1.0	75.0	77.0	0.97
250x75x18x1.9	245.0	1.90	515	1.0	69.4	75.0	0.93
160x65x15x1.9	156.8	1.92	515	1.0	73.8	70.5	1.05
200x75x15x1.5	197.0	1.51	537	1.0	57.0	54.5	1.05
250x75x18x1.5	247.3	1.49	537	1.0	53.2	55.0	0.97
160x65x15x1.5	157.5	1.51	537	1.0	54.5	53.5	1.02
120x50x18x1.5	116.8	1.49	537	1.0	43.3	45.4	0.95
200x75x15x1.95	198.0	1.93	271	1.0	55.1	50.0	1.10
250x75x18x1.95	248.3	1.94	271	1.0	60.3	57.0	1.06
160x65x15x1.95	158.0	1.94	271	1.0	52.2	48.0	1.09
120x50x18x1.95	118.6	1.95	271	1.0	38.1	37.4	1.02
Mean							1.02
COV							0.057

Note: d_1 = flat portion of clear height of web, f_{yw} = web yield stress, t_w = web thickness, a = shear span, and a/d_1 = aspect ratio.

Table 11: Ultimate Shear Capacities of LSBs in the DSM Format (Tests and FEA)

LSB Sections $dxb_fxd_fxt_w$	Shear Capacity V_v (kN)				V_{cr} (kN)	V_y (kN)	λ	V_V/V_y	
	Test	FEA	AS/NZS 4600	Eqs. (10) to (13)				Test	FEA
150x45x15x2.0	68.5	70.0	66.1	62.0	140.57	62.00	0.66	1.10	1.13
200x45x15x1.6	63.6	63.5	41.6	57.2	54.29	74.07	1.17	0.86	0.86
200x60x20x2.0	88.2	88.5	71.2	78.0	105.43	83.29	0.89	1.06	1.06
200x60x20x2.5	119.3	118.0	114.2	107.1	214.13	107.06	0.71	1.11	1.10
250x60x20x2.0	90.1	93.0	60.7	85.2	79.26	111.39	1.19	0.81	0.83
250x75x25x2.5	139.6	136.5	116.4	127.2	173.58	135.01	0.88	1.03	1.01
300x60x60x2.0	93.0	96.0	49.3	83.9	64.31	142.52	1.49	0.65	0.67
300x75x25x2.5	143.7	151.5	106.9	136.1	139.56	169.09	1.10	0.85	0.90
125x45x15x2.0	56.9	56.0	52.5	49.2	144.23	49.25	0.58	1.16	1.14
150x45x15x1.6	45.8	47.8	40.6	47.4	61.81	51.67	0.91	0.89	0.93
150x45x15x1.6	47.1	47.8	40.6	47.4	61.81	51.67	0.91	0.91	0.93
150x45x15x1.6	47.0	47.8	40.6	47.4	61.81	51.67	0.91	0.91	0.93
150x45x15x2.0	61.1	61.0	60.9	59.9	119.82	59.94	0.71	1.02	1.02
150x45x15x2.0	58.8	61.0	60.9	59.9	119.82	59.94	0.71	0.98	1.02
150x45x15x2.0	59.5	61.0	60.9	59.9	119.82	59.94	0.71	0.99	1.02
200x45x15x1.6	56.8	55.0	31.7	53.2	46.27	74.07	1.27	0.77	0.74
200x45x15x1.6	54.2	55.0	31.7	53.2	46.27	74.07	1.27	0.73	0.74
200x60x20x2.0	74.0	76.0	61.6	73.7	89.86	83.29	0.96	0.89	0.91
200x60x20x2.5	110.0	109.0	100.5	107.1	182.51	107.06	0.77	1.03	1.02
250x60x20x2.0	>75.0	83.0	46.3	78.5	67.56	111.39	1.28	N/A	0.75
250x75x25x2.5	118.9	121.0	101.4	120.1	147.95	135.01	0.96	0.88	0.90
300x60x20x2.0	> 75.0	82.0	37.6	76.7	54.81	142.52	1.61	N/A	0.58
300x75x25x2.5	125.1	131.0	81.5	128.9	118.95	169.09	1.19	0.74	0.77
200x60x20x2.0	79.4	75.0	59.7	73.1	88.13	83.29	0.97	0.95	0.90
200x60x20x2.5	107.9	106.0	98.9	107.1	179.00	107.06	0.77	1.01	0.99

Note: d_1 = flat portion of clear height of web, f_{yw} = web yield stress, t_w = web thickness, a = shear span, a/d_1 = aspect ratio, V_{cr} = Elastic shear buckling capacity, V_y = Shear yielding capacity

Table 12: Ultimate Shear Capacities of LCBs in the DSM Format (Tests and FEA)

LCB Sections	Shear Capacity V_v (kN)				V_{cr} (kN)	V_y (kN)	ƛ	V_V/V_y	
	Test	FEA	AS/NZS 4600	Eqs. (10) to (13)				Test	FEA
200x75x15x1.9	75.0	77.0	60.7	75.8	65.6	116.9	1.34	0.64	0.66
250x75x18x1.9	69.4	75.0	47.3	69.6	51.1	143.8	1.68	0.48	0.52
160x65x15x1.9	73.8	70.5	73.2	75.6	82.4	93.0	1.06	0.79	0.76
200x75x15x1.5	57.0	54.5	29.5	44.7	31.9	95.8	1.73	0.59	0.57
250x75x18x1.5	53.2	55.0	22.6	43.3	24.4	118.7	2.21	0.45	0.46
160x65x15x1.5	54.5	53.5	37.0	47.2	39.9	76.6	1.39	0.71	0.70
120x50x18x1.5	43.3	45.4	45.0	46.3	51.7	56.1	1.04	0.77	0.81
200x75x15x1.95	55.1	50.0	53.6	54.2	66.2	62.1	0.97	0.89	0.80
250x75x18x1.95	60.3	57.0	49.7	57.9	53.6	78.3	1.21	0.77	0.73
160x65x15x1.95	52.2	48.0	53.2	49.9	84.7	49.9	0.77	1.05	0.96
120x50x18x1.95	38.1	37.4	40.1	37.6	114.1	37.6	0.57	1.01	0.99

Note: d_1 = flat portion of clear height of web, f_{yw} = web yield stress, t_w = web thickness, a = shear span, a/d_1 = aspect ratio, V_{cr} = Elastic shear buckling capacity, V_y = Shear yielding capacity

Table 13: Ultimate Shear Capacities of Plate Girders in the DSM Format (Tests) [20]

PG Sections	d_1 (mm)	a/d_1	t_w (mm)	t_f (mm)	t_f/t_w	b_f (mm)	f_{yf} (MPa)	f_{yw} (MPa)	V_y (kN)	V_{cr} (kN)	V_V (kN)	λ	V_V/V_y
G1	400	1.0	4	15	3.75	130	303.8	318.5	305.8	346.0	282.4	0.94	0.92
G2	600	1.0	4	10	2.50	200	303.8	318.5	458.6	230.7	332.5	1.41	0.72
G3	600	1.0	4	15	3.75	200	303.8	318.5	458.6	230.7	337.4	1.41	0.74
G4	400	1.5	4	15	3.75	130	303.8	318.5	305.8	293.4	268.8	1.02	0.88
G5	600	1.5	4	10	2.50	200	303.8	318.5	458.6	195.6	286.4	1.53	0.62
G6	600	1.5	4	20	5.00	200	303.8	318.5	458.6	195.6	312.8	1.53	0.68
G7	600	2.0	4	10	2.50	200	303.8	285.2	410.7	181.0	258.9	1.51	0.63
G8	600	2.0	4	15	3.75	200	303.8	285.2	410.7	181.0	276.5	1.51	0.67

Note: d_1 = flat portion of clear height of web, f_{yw} = web yield stress. f_{yf} = flange yield stress, t_w = web thickness, t_f = flange thickness, a = shear span, a/d_1 = aspect ratio, V_{cr} = Elastic shear buckling capacity, V_y = Shear yielding capacity